

ICSV14
Cairns • Australia
9-12 July, 2007



NUMERICAL INVESTIGATION OF AERODYNAMIC SOUND RADIATED FROM A BLUFF BODY USING Lighthill Tensor

Shoji Kato¹, Hiroshi Muraoka², Yuta Takahashi², Tubagus Haedar², and Akiyoshi Iida¹

¹Kogakuin University, 2665-1 Nakanomachi, Hachioji-shi, Tokyo, 192-0015, Japan
skato@iis.u-tokyo.ac.jp (email address of lead author)

²Research Center of Computational Mechanics, Inc.
Togoshi NI-Bldg. 1-7-1 Togoshi, Shinagawa-ku, Tokyo, 142-0041, Japan
actran@rccm.co.jp (email address of lead author or presenter)

Abstract

Verifying the effectiveness of Lighthill tensor's application coupled with both Finite Element Method (FEM) and Infinite Element Method (IEM) for aero acoustic scattering analysis was the main purpose of this research. The Lighthill tensor is classified as the real source of aerodynamic sounds being generated within a fluid domain and understanding its nature is critical in terms of noise reduction during a product development phase. In order to evaluate both sound pressure strength and propagation pattern, aeroacoustic fields surrounding a rectangular cylinder placed in a uniform flow was tested. Lighthill tensor was taken from CFD (Front Flow/Blue, FLUENT) calculation and the outcome was compared to ones using Boundary Element Method (BEM) analysis based on reduced Curle's equation along with wind tunnel experimental data. The main sound source was seen near the trailing edge of the cylinder at approximately 1-2 times the length of the rectangle's side. Although significant margins between the three methods were observed at low frequency, beyond 100Hz, the characteristic of sound pressure strength were closely matched. It became evident that if consideration regarding directivity or the aerodynamic sound source scattering needed to be taken into account, ACTRAN (Lighthill tensor calculation in the domain) application was more prominent than utilizing reduced Curle's equation (pressure on the surface).

1. INTRODUCTION

One of the major problems in our society is noise pollution and no matter where the sound originates, it is essential to understand how it is created, in order to control the magnitude of its effect. Commonly, the calculation of the flow and sound fields are carried out separately as the relative scaling for the two domains differs. Also, it is stated that the aerodynamic sound is proportional to the flow velocity order of 6th to 8th power.

Aero acoustic noise is generated from vortices created when a fluid makes contact with a solid object in a flow field, in this paper a rectangular cylinder. Direct Numerical Simulation (DNS) [1] was the obvious approach to aero acoustics related to compressible Navier-Stokes equations however, due to its calculation cost being proportional to Re^3/M^4 , its use was limited

to low Reynolds number flow. Similarly, application of BEM does have advantages in terms of reduced dimensionality, however, as its principle can only take into account the surface pressure from an object, it ends to be limited for dipole analysis problems. Curle's equation [2] or the compact Green's functions are effective under compact problem (size of the propagated wavelength is considerably larger than the size of the object) when diffraction effect is non-existent.

On the contrary, the FEM domain-based methods such as FEM/IEM [3] are more suitable for solving exterior acoustic problems due to its sparse matrices and efficient solution procedures such as parallel calculations along with enabling a natural extension of finite element to an unbounded domain. Geometrical complexity does not bear any effect on the efficiency as it is based on the weak variational formulation and sound hard condition is automatically accounted as a natural boundary condition. Although the FEM offers high accuracy results, it should be noted that the computational load is heavy due to the need of discretization of the whole computational domain (large stiffness matrix).

Lighthill's approach [4] is one, where the aerodynamic source is first estimated using its analogy from the flow results then using it to accurately obtain the true propagation of the acoustic wave. The corresponding aerodynamic sound sources were obtained by CFD analysis [5] under large eddy simulation (LES) with dynamic Smagorinsky model. Coupling this analogy with FEM/IEM (see figure 1) enables to facilitate the calculation of volumetric sound propagation with high accuracy and constraining the infinite boundary around the noise source culminates in reducing calculation time and cost respectively. Alternatively, the Powell sound source (product of vorticity magnitude and velocity) taken from CFD calculation could replace the Lighthill tensor for acoustic calculation. A square cylinder (side length of 0.02m) was placed in a uniform flow at varying angles of attack (0 to 45 degrees) to determine its turbulent nature. Essentially, outlining differences between compact (BEM) and non-compact (FEM) sound was the aim of this paper.

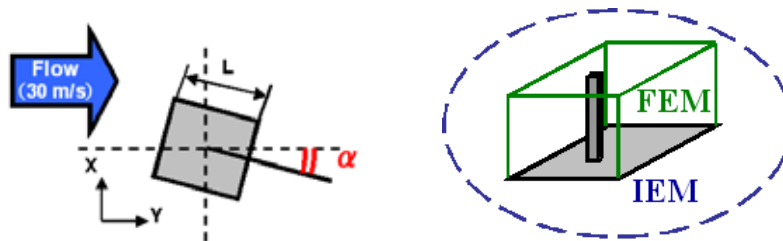


Figure 1. Square cylinder and its FEM/IEM boundary separation

This paper is organized as follows: After this introduction, the acoustic analogy is presented in section 2. Section 3 outlines the square cylinder problem definition and both numerical and contour results are compared in section 4. The penultimate section illustrate a similar approach used on a side mirror of a car and the final sections summarize the validity of this research indicating plausible steps for further studies.

2. ACOUSTIC ANALOGY

First the continuity (1) and Navier-stokes (2) equations are considered.

$$\frac{\partial \rho}{\partial t} + \frac{\partial \rho v_i}{\partial x_i} = 0 \quad (1)$$

$$\frac{\partial \rho v_i}{\partial t} + \frac{\partial \rho v_i v_j}{\partial x_j} = -\frac{\partial (p \delta_{ij} - \tau_{ij})}{\partial x_j} \quad (2)$$

Continuity is differentiated by t and sound terms are added to Navier-Stokes. Following this, equation (2) is differentiated by x_i and combining with equation (1) provides the following.

$$\frac{\partial^2 (\rho - \rho_0)}{\partial t^2} - a_0^2 \frac{\partial^2 (\rho - \rho_0)}{\partial x_i \partial x_i} = \frac{\partial^2}{\partial x_i \partial x_j} [\rho v_i v_j + \delta_{ij} (p - a_0^2 \rho) - \tau_{ij}] \quad (3)$$

The fluctuation density is represented by $(\rho - \rho_0)$, where ρ_0 is the mean or atmospheric density and a_0 denotes the speed of sound. Placing the Lighthill tensor (T_{ij}) term on the right hand side of equation (3) will define the Lighthill's equation.

$$\frac{\partial^2 (\rho - \rho_0)}{\partial t^2} - a_0^2 \frac{\partial^2 (\rho - \rho_0)}{\partial x_i \partial x_i} = \frac{\partial^2 T_{ij}}{\partial x_i \partial x_j} \quad (4)$$

The weak variational form of equation (4) is applied in ACTRAN [6] as derived by Oberai et al [7,8].

$$\int_{\Omega} \left(\frac{\partial^2}{\partial t^2} (\rho - \rho_0) \delta \rho + a_0^2 \frac{\partial}{\partial x_i} (\rho - \rho_0) \frac{\partial \delta \rho}{\partial x_i} \right) dx = - \int_{\Omega} \frac{\partial T_{ij}}{\partial x_j} \frac{\partial \delta \rho}{\partial x_i} dx + \int_{\Gamma} \frac{\partial \Sigma_{ij}}{\partial x_j} n_i \delta \rho d\Gamma(x) \quad (5)$$

The two terms on the right hand side of equation (5) is comprised by volumetric and surface aerodynamic source respectively, where $\delta \rho$ is a test function, Ω denotes the computational domain and Γ represent the surface boundary. In a far field, acoustic pressure p_a can be represented as follows.

$$p_a(x, t) = a_0^2 (\rho - \rho_0)(x, t) \quad (6)$$

Hence aerodynamic sound propagated in a flow field with solid boundary can be defined by the following Curle's equation (7), where P is the pressure, T_{ij} is the Lighthill tensor and S represents the solid object's surface. In addition, x represents the observation point, y is the location of the sound source, n_i is the normal vector from the boundary and r denotes the distance between the source and the recipient.

$$p_a(x, t) = \frac{1}{4\pi} \frac{\partial^2}{\partial x_i \partial x_j} \int_V \frac{T_{ij}(y, t - r/a_0)}{r} d^3 y - \frac{1}{4\pi} \frac{\partial}{\partial x_i} \int_S \frac{n_i P(y, t - r/a_0)}{r} dS \quad (7)$$

Under low Mach number flow field, the first term on the right of equation (7), which corresponds to quadrupole sound source can be neglected in relation to the second term (dipole sound source). If the object scale is considerably smaller compared to the wavelength of the sound source, the dipole term's space differential is converted to time differential resulting into what we define as the reduced Curle's equation (8). In this instant r represent the distance

between the receiver and the centre of the solid object.

$$p_a(x,t) = -\frac{1}{4\pi a_0} \frac{x_i}{r^2} \frac{\partial}{\partial t} \int_S n_i P(y,t-r/a_0) dS \quad (8)$$

By defining the Lighthill's tensor within the Helmholtz equation (solved in the frequency domain), the surrounding sound pressure distribution around the square cylinder and directivity can be determined.

3. NUMERICAL CONDITIONS

Two separate meshes suitable for flow and acoustic analysis were created to facilitate the evaluation process in terms of capturing the vorticity nature of the flow field and the resulting sound wave propagation nature respectively. The flow field mesh comprised of 2.9 million elements and the Reynolds number was set to 40000 as illustrated below. Also, the LES calculation results were used as a base for the reduced Curle's equation application to obtain the acoustic feature derived from surface pressure fluctuation.

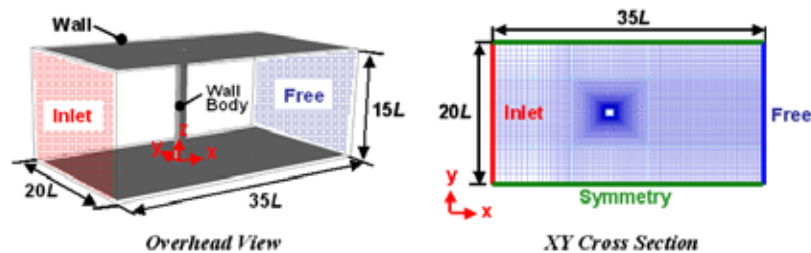


Figure 2. Aerodynamic boundary condition and grid structure

Five angles of attacks for the cylinder were tested (0, 10, 15, 30 and 45 degrees) and the spanwise length of the cylinder was set 15 times the side length of the square. Boundary conditions were placed as to recreate the wind tunnel setting and LES was applied to obtain the Lighthill tensor necessary for acoustic studies. Dimensions of the analysis domain and cylinder remained unchanged, however the density of the mesh was reduced to 200000 elements as shown in figure 3.

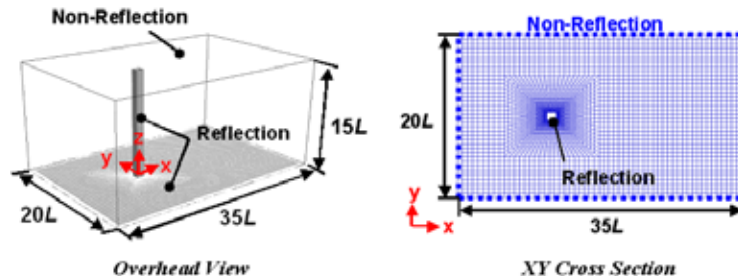


Figure 3. Acoustic boundary condition and grid structure

Unlike the aerodynamic mesh, the acoustic mesh does not need similar density as long as the elements size are small enough to capture the wavelength of the relevant frequency. Non-reflective boundary (IE) was placed for the surrounding except for the floor and cylinder which

had the wall property (reflective boundary). Acoustic simulations were carried out across varying Strouhal numbers ($St = fL/U$) having relative frequencies between 49.5Hz to 2734.5Hz in the goal of evaluating sound propagation nature, directivity, peak frequency component and general efficiency of the three different methods.

4. RESULTS AND COMPARISON

LES analysis illustrated that as the angle of attack attain 15 degrees, the separated flow re-attaches at the bottom of the cylinder which decreases the sound source strength behind and on the surface of the solid object as shown in figure 4. This indicates that the propagating vorticity phase is not symmetric between the top and bottom of the cylinder at this particular angle contrary to the others.

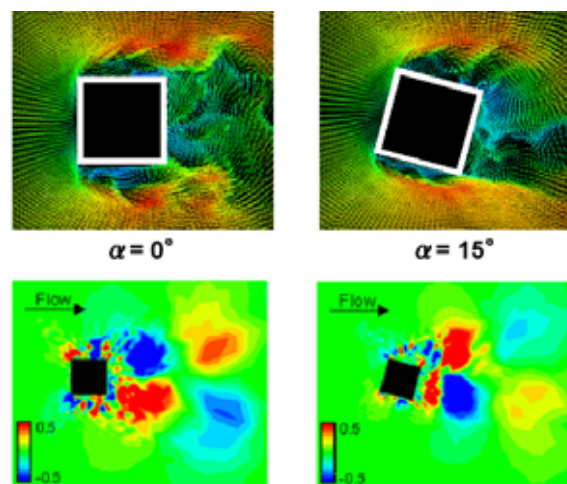


Figure 4. Velocity vector and Lighthill tensor distribution ($\log |T_{ij}|$) around the cylinder

In essence the directivity will always be in a dipole shape when the reduced Curle's equation is applied. Figure 5 reiterates that under similar analysis using a commercial BEM code, the directivity is hardly affected by the angle of attack of the cylinder since the analysis can be assumed as being a compact body having no diffraction effects.

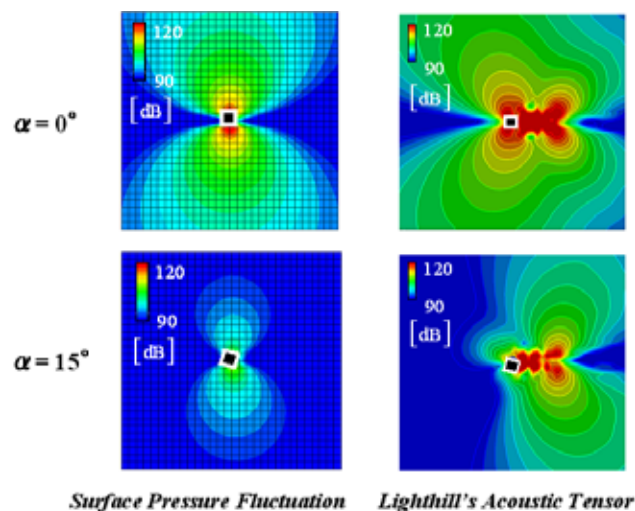


Figure 5. Distribution of sound pressure radiated from a square cylinder ($St = 0.13$)

In contrast, as the Lighthill tensor represents the vorticity movement of the flow, the directivity illustrate a quadrupole and dipole characteristics under FEM conditions with a compact body. Analysis method's efficiencies (reduced Curle's equation, FEM, wind tunnel experiment) were compared using the sound pressure level obtained from a point 1m lateral (Y direction) to the square cylinder as demonstrated in Figure 6.

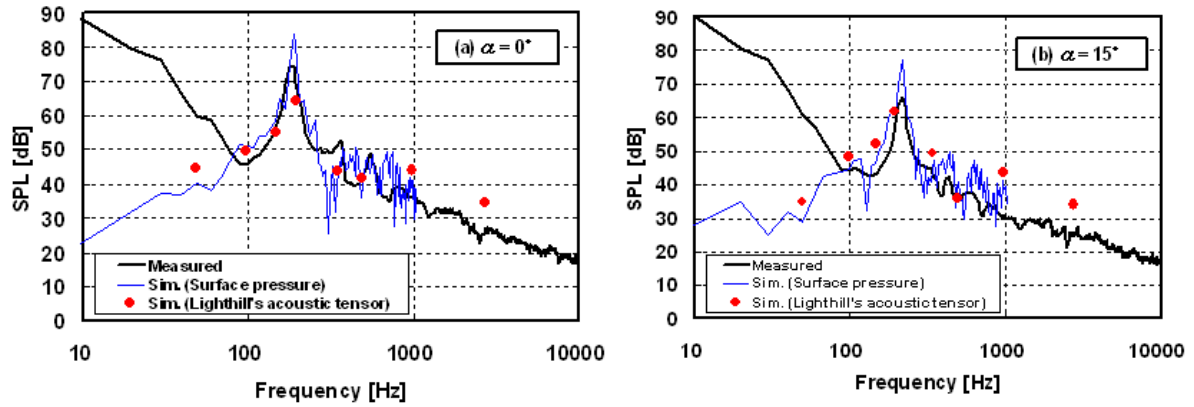


Figure 6. Sound pressure level comparison between angle of attack at 0 degree and 15 degrees

Both graphs have similar curve patterns in terms of sound pressure fluctuation including the peak frequency at around 200Hz ($St = 0.13$) and except for the lower frequency region; all three methods were within ± 10 dB of each other. The miss alignment between the experimental and numerical analysis methods below 100Hz was probably due to the background noise created within the wind tunnel. Following these results, a slightly more complex geometry was tested using the Lighthill tensor application to investigate the directivity fluctuation.

5. FURTHER STUDY

A side mirror of height 0.3m and 0.1m radius was placed in a uniform flow field of 55m/s for LES calculation using FLUENT. Grid structures for both flow and sound analysis are shown below.

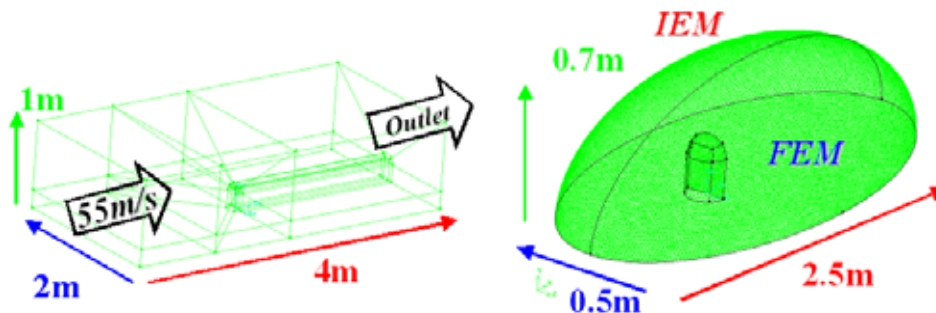


Figure 6. Aerodynamic and Acoustic mesh dimensions

Similar to the square cylinder case, the acoustic mesh (approximately 600000 elements) was less dense compared to the aerodynamic mesh comprising of 2.8 million elements. Although the frequency was set at 1000Hz (wavelength of 0.34m), the element size was small enough to

accommodate up to 2500Hz in order to maximize the calculation efficiency. IE were placed on the ellipsoidal surface of the acoustic grid.

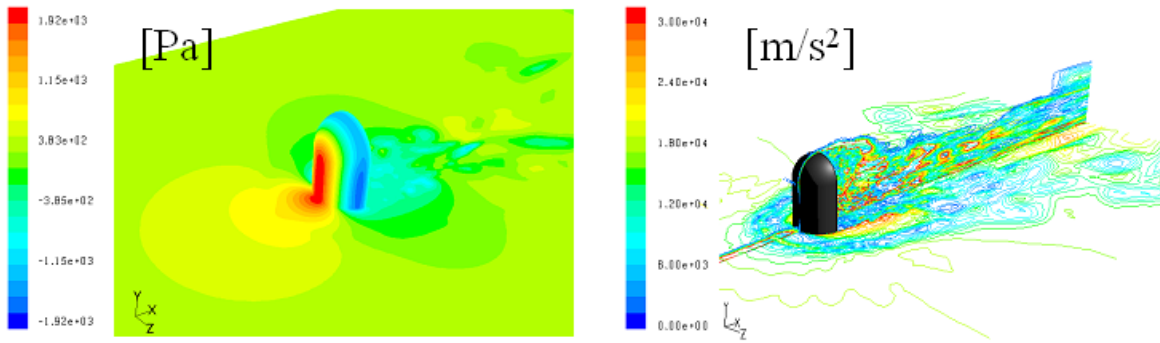


Figure 7. Pressure and Powell sound source contours from FLUENT

Approximately 20000 iterations were carried out ($\Delta t = 6 \times 10^{-5}$) to determine the wake characteristics and the corresponding Lighthill tensor around the side mirror shown in figure 7. Applying this into ACTRAN provided contours seen in figure 8, where the sound seemed to be propagating from a point behind the mirror.

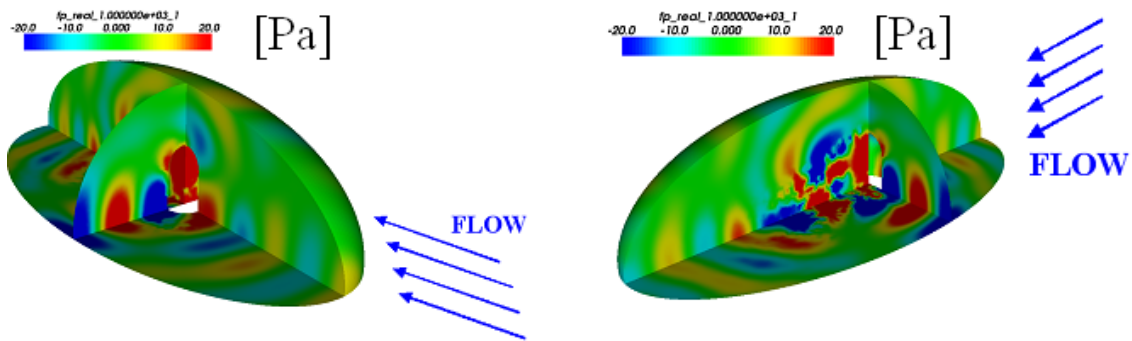


Figure 8. Sound wave propagation by the side mirror (front and rear view)

Maximum sound pressure level was calculated to be around 135dB and the high noise region is mainly concentrated at the back of the mirror. It is also evident that sound pressure strength was diminished towards the front side as the mirror surface diffracted the oncoming waves as illustrated in figure 9.

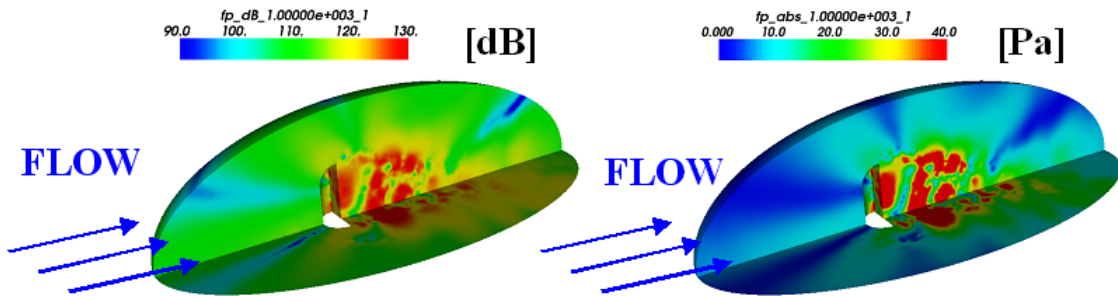


Figure 9. Sound pressure level and Amplitude contour (side view)

6. CONCLUSIONS

Sound was generated from the rear of the cylinder at approximately one to twice the side length of the rectangular cylinder following LES calculation and the application of Lighthill tensor allows the proper visualization of sound directivity and sound wave distribution. When the cylinder was at angle of attack of 15 degrees, the re-attachment of the separated flow culminated in a reduction effect upstream of the cylinder in both directivity and diffraction. FEM provided both quadrupole and dipole directivity characteristic at varying angles unlike the reduced Curle's equation cases where it continuously generated dipole nature. However, all three methods showed similarity in terms of numerical output concerning sound pressure levels across variable frequency range especially for the peak frequency value, which stayed constant regardless of the angle of the cylinder at around 200Hz. It is therefore valid to state that compact (BEM) and non-compact (FEM) sound source do not differ in terms of numerical result, hence the application would be dependent on whether it is necessary to account for the sound source's dynamic movement and the accurate capturing of directivity pattern. As a suggestion to further cement this finding, the case could be analysed at a small angle of attack and frequency increment along with other calculation methods for result refinement. Applying a more complex geometry will also be investigated.

REFERENCES

- [1] C. Kato, M. Kaiho, and A. Manabe, "*Industrial Application of LES in Mechanical Engineering*" (invited paper), DNS/LES Progress and Challenges, pp. 47-58, Greyden Press (2001-11).
- [2] N. Curle, "The influence of Solid Boundaries on Aerodynamic Sound", *Proc. Roy. Soc (London)*, Volume A 231, No. 1187, pp. 505-514 (1955).
- [3] R.J. Astley, G.J. Macaulay and J.P. Coyette, "Mapped wave envelope elements for acoustic radiation and scattering", *JSV*, 170 (1), 97-118 (1994)
- [4] M.J. Lighthill, *Waves in fluids*, CAMBRIDGE UNIVERSITY PRESS, 1978.
- [5] K. Ohnishi, H. Zhang, T. Tomohiro, H.Kayama, Kamisu-cho, M.Nawa, N.Taniguchi, "*The evidence of the noise analysis technique by LES using general-purpose code FrontFlow*," *JFSM*, Vol. 18, (2004)
- [6] Free-Field-Technologies-S.A., *Actran 2006 Aeroacoustic Solutions: Actran/TM and Actran/LA - User's Manual*, Belgium, 2006.
- [7] A. Oberai, F. Ronaldkin and T. Hughes, "Computational Procedures for Determining structural-Acoustic Response due to Hydrodynamic Sources", *Comput. Methods Appl. Mech. Engrg*, Volume 190, pp. 345-361 (2000).
- [8] A. Oberai, F. Ronaldkin and T. Hughes, "Computation of Trailing-Edge Noise due to Turbulent Floe over an aerofoil", Volume 40, pp. 2206-2216 (2002).
- [9] M.S. Howe, *Theory of Vortex Sound*, CAMBRIDGE UNIVERSITY PRESS, 1992.